

Reentrant Orbital Order and the True Ground State of $\text{LaSr}_2\text{Mn}_2\text{O}_7$

Qing'An Li,^{1,2} K.E. Gray,^{2,*} H. Zheng,² H. Claus,² S. Rosenkranz,² S. Nyborg Ancona,² R. Osborn,² J.F. Mitchell,² Y. Chen,^{3,4} and J.W. Lynn³

¹Chinese Academy of Sciences, Beijing, CHINA

²Materials Sciences Division, Argonne National Laboratory, Argonne, IL 60439, USA

³NIST Center for Neutron Research, National Institute of Standards and Technology, Gaithersburg, MD 20899, USA

⁴Department of Materials Science and Engineering, University of Maryland, College Park, MD 20742, USA

(Dated: October 23, 2021)

Contrary to conventional wisdom, our purified $\text{La}_{2-2x}\text{Sr}_{1+2x}\text{Mn}_2\text{O}_7$ crystals exhibit *CE*-type orbital and charge order as the low-temperature ground state for a hole doping level $h = 0.5$. For small deviations from $h = 0.5$, the high temperature *CE* phase is replaced at low temperatures by an *A*-type antiferromagnet without coexistence. Larger deviations result in a lack of *CE* order at any temperature. Thus, small inhomogeneities in cation or oxygen composition could explain why others commonly see this reentrance with coexistence.

The quest to better understand strongly correlated electrons is at the heart of condensed matter inquiry. Colossal magnetoresistive manganites exhibit a particularly vigorous competition among orbital, charge and spin order [1, 2]. The phase diagrams, e.g., $\text{La}_{1-x}\text{Sr}_x\text{MnO}_3$ or the bilayer version $\text{La}_{2-2x}\text{Sr}_{1+2x}\text{Mn}_2\text{O}_7$, display interesting features near half doping ($x \sim 0.5$) where, e.g., long-range orbital and “checkerboard” charge ordering (*CE* type) is predicted [3]. In bilayer manganites, it has been commonly accepted that *CE* order at $x = 0.5$ is reentrant [4, 5, 6, 7, 8, 9, 10]: it forms below ~ 210 K, but then is replaced by an *A*-type antiferromagnet (AAFM) below ~ 100 K. The lack of a low-temperature *CE* ordered ground state is surprising as it is found at $x = 0.5$ in many perovskite manganites [11]. In bilayer manganites, coexistence of *CE* order and AAFM between ~ 100 K and ~ 200 K is also universally reported [4, 5, 6, 7, 9].

All reports of reentrance in $\text{LaSr}_2\text{Mn}_2\text{O}_7$ are based on superlattice peaks in neutron [4, 5, 6, 7], x-ray [6, 7, 8, 9, 10] and electron [12, 13, 14] diffraction and/or a peak in the resistivity [4, 6, 8, 12]. However, consistent with our own experience, these reported properties for $x = 0.5$ doping are variable. This implies an exquisite sensitivity to the exact value of hole doping, $h = x - \delta$ in $\text{La}_{2-2x}\text{Sr}_{1+2x}\text{Mn}_2\text{O}_{7-\delta}$. This dictates a vital burden to obtain sample uniformity. Thus, in the present study we have purified large single crystals, which often exhibit compositional gradients, by cleaving them into very small crystals (~ 1 mg) and discarding those that do not pass our test for uniformity (see below). Combining conductivity, magnetization, and neutron and high-energy x-ray diffraction data on such highly homogeneous crystals, we here show that the *CE* order predicted by Goodenough [3] is the low-temperature ground state, presumably at $h = 0.5$, and that coexistence of *CE* and AAFM order is absent. We argue that re-entrance only occurs for small deviations from 0.5 and propose a revised phase diagram for bilayer manganites near $h = 0.5$.

Crystals were melt-grown in an optical image furnace [15]. The *c* axis is perpendicular to the platelike crystals ($\sim 2 \times 0.5 \times 0.1$ mm³) and four gold pads are deposited along the top and bottom surfaces for transport measurements. In order to obtain a direct measure of the different order parameters, we performed high-energy synchrotron X-ray scattering experiments at the 1-ID-C station of the Advanced Photon Source at Argonne National Laboratory and neutron scattering experiments at the BT-7 triple-axis instrument at the NIST Center for Neutron Research. We utilize the (9/4,1/4,0) reflection obtained using 80 keV X-rays and the neutron intensities of the (1/4,1/4,3) and (1,1,3) reflections as measures of the *CE* orbital order, the *CE* antiferromagnetic order (CEAFM), and the *A*-type antiferromagnetic order, respectively [4].

Since four-terminal methods are unreliable for bulk crystals, we use six terminals to determine each principal component of conductivity, i.e., along the *c*-axis, σ_c , and in the *ab*-plane, σ_{ab} [16]. In transport method *A*, current is injected through the outermost contacts on one surface [Fig. 1(a)]. Laplace’s equation is solved and inverted to get σ_{ab} and σ_c from voltages measured across the innermost contacts of each surface. In method *B*, Laplace’s equation is solved for current injection through the top and bottom contacts at one end of the crystal, while voltages are measured between pairs of contacts on the top and bottom of the crystal [Fig. 1(b)].

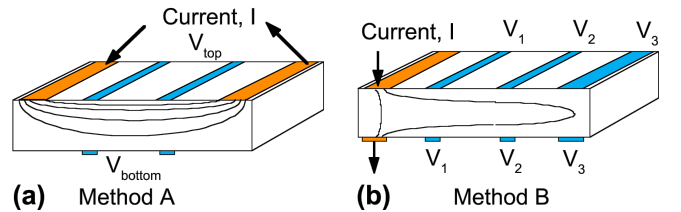


FIG. 1: Schematic of six-terminal configurations for method *A* (a) and method *B* (b).

To test for homogeneity, we evaluate σ_{ab} and σ_c in four configurations. Two use method *A* with current applied to the outer contacts of either the top or bottom surfaces and two use method *B* with current applied to the end contacts on either the right- or left-hand sides. We require both $\sigma_{ab}(T)$ and $\sigma_c(T)$ to be qualitatively the same for all four configurations and within a factor of 2-3 in magnitude. Crystals used for Fig. 2 and 3 all pass our criteria, as described in Ref. [17]. Homogeneous crystals with a nominal $x = 0.5$ fall into three batches: batch-*A* are reentrant, batch-*B* exhibits *CE* order as the predominant low-temperature ground state, and batch-*C* never exhibit *CE* order. Examples of these are indicated in the highly schematic phase diagram of Fig. 4. The fact that we see three, and only three, *unique* states using four

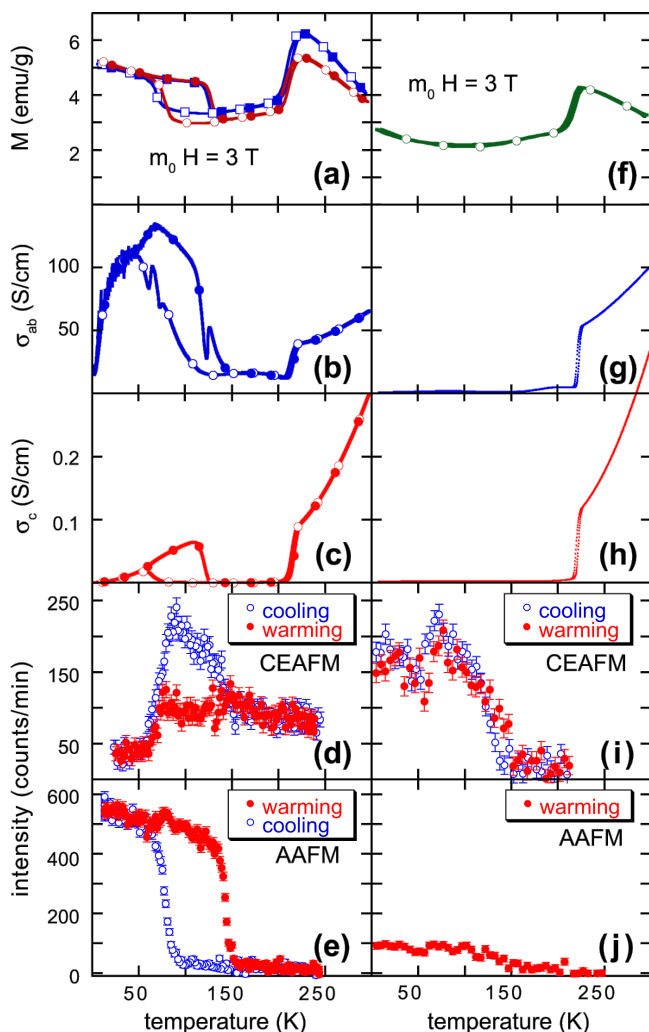


FIG. 2: Temperature dependence, shown for reentrant crystals (a)–(e) and nonreentrant crystals (f)–(j), of magnetization (a),(f), conductivity in ab -plane (b),(g) and along c -axis (c),(h) and neutron diffraction for CEA FM (d),(i) and A-type AFM (e),(j). Open symbols refer to cooling and filled symbols to warming.

different bulk probes is unmistakable evidence of sufficient compositional uniformity. Any broad distribution of $h = x - \delta$ would result in the coexistence of these states in some of the 12 crystals studied. The relevance of δ is seen in one reentrant crystal that transformed into a non-reentrant crystal after annealing in pure oxygen for 60 hrs at 600 °C. Our scattering probes show that our samples consist of up to two or three slightly misaligned crystallites but are free from any impurity phases within our detection limits.

Most of our crystals of nominal $x = 0.5$ composition display a transition from a paramagnetic insulator (PMI) above ~ 200 K into a *CE*-type orbital and charge ordered state. This is often (batch-*A*) followed by a hysteretic transition into a state with higher magnetization [Fig. 2(a)] and conductivity [Figs. 2(b) and 2(c)] below ~ 100 K that does not exhibit the *CE*-type superlattice reflections [Figs. 2(d) and 3]. Our neutron diffraction data [Fig. 2(e)] confirm that the low-temperature state is the previously identified AAFM [4, 5, 6, 7]. However, in several crystals (batch-*B*) no more than a few percent [Figs. 2(f)–2(j)] transformed into the AAFM. A natural explanation is that *CE* order is the stable ground state only over a very narrow range of h and there are crystal-to-

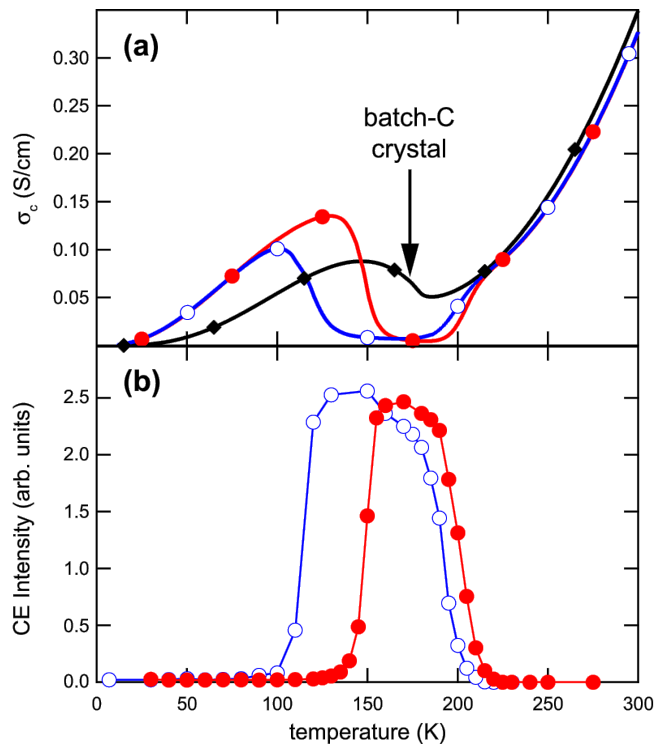


FIG. 3: Temperature dependencies of (a) σ_c and (b) x-ray diffraction intensity of the superlattice reflection for *CE* order (9/4,1/4,0), measured on the same crystal. Reentrance and hysteresis show a perfect correlation upon cooling (open symbols) and warming (filled symbols). Also shown in (a) are the conductivity data (black diamonds) for a batch-*C* crystal.

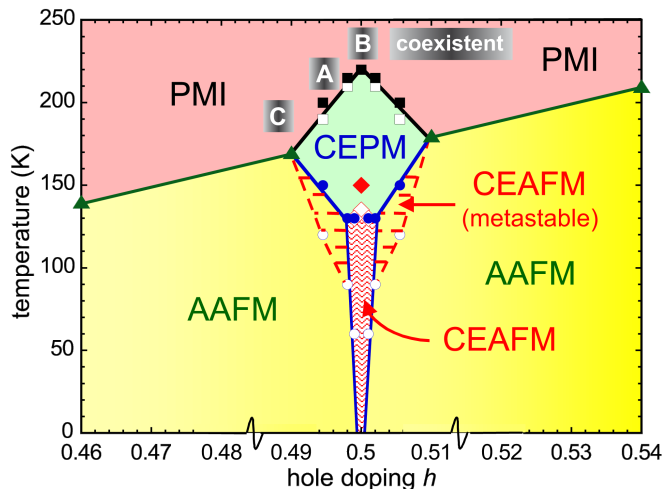


FIG. 4: Schematic, qualitative phase diagram near $h = 0.5$. Symbols are measured transition temperatures (open: cooling; filled: warming). Except for $h = 0.46$ and 0.54 , the h values are arranged to connect smoothly with other data since we cannot determine them with sufficient precision. Reentrant crystal data are plotted symmetrically both above and below 0.5 . The metastable CEA FM is found on cooling but not on warming. The width of the boxes labeled coexistent, A, B, and C represent suggested range of h -values (i.e., $\langle h \rangle \pm \Delta h$) for coexistent crystals and batches A, B and C.

crystal variations of the average hole doping $\langle h \rangle$ and a finite width of the distribution Δh . Thus, when $\langle h \rangle$ is most favorable for CE order, presumably at 0.5 as predicted by Goodenough [3], a larger fraction of the crystal would exhibit the CE ground state at low temperatures. Then for sufficiently small Δh , the CE ground state can be the majority phase. For crystals exhibiting re-entrance we believe $\langle h \rangle$ differs somewhat from 0.5 . We also find crystals (batch-C) without a transition to the CE -state, implying that $\langle h \rangle$ is yet further from 0.5 . The conductivity data for batch-C crystals are very similar to that of Ref. [18] and are shown in Fig. 3(a) for a nominal doping $x = 0.48$. Note that the sharp decrease in σ_c at ~ 200 K, found in the reentrant and nonreentrant crystals, is entirely absent, and the conductivity changes directly from the PMI to the AAFM behavior.

Data on batch-A crystals display a striking temperature dependence and hysteresis in σ_{ab} and σ_c and magnetization, as shown in Figs. 2(a)-2(c) and 3(a). Similar hysteresis is also found in the diffraction data of Figs. 2(d), 2(f) and 3(b) and in the data of others [4, 7]. Such hysteresis was also reported in resonant x-ray studies [9], but we are unaware of reports of such dramatic hysteresis in the conductivity or magnetization of $\text{LaSr}_2\text{Mn}_2\text{O}_7$. The drops in our conductivity and magnetization data exhibit a similar temperature range and hysteresis as all the published diffraction data [4, 7, 9]. A striking conclusion of our neutron diffraction data for this batch-A crystal is the lack of coexistence of CE and AAFM order,

which is universally found by others [4, 6, 7]. Neutrons probe AAFM and CEA FM magnetic order [Figs. 2(d) and 2(e)], the latter of which only occurs below ~ 130 K (above 130 K the CE state is paramagnetic). In warming and cooling cycles, one, and only one, state is ever found. This conclusion is possible because of the small Δh in our crystals. Near the lower-temperature transition of batch-A crystals, we found evidence for sluggish kinetics that was assisted by magnetic fields of 7 T. This may imply a small energy difference between these states since the change in magnetization at the transition is only ~ 2 emu/g. Further, the broad thermal hysteresis associated with reentrance implies there is only a slight difference in the temperature dependencies of their free energies.

Crystals from batch-B exhibit a similar high-temperature transition, but only a trace of the lower temperature transition to AAFM states. This is clearly seen in magnetization [Fig. 2(f)] and conductivity [Figs. 2(g) and 2(h)]. Apparently the free energy for CE order, that is the majority phase of batch-B crystals, is sufficiently low so that CE order remains stable down to low temperatures. Since CE order has a sharp minimum in its free energy for h exactly 0.5 , batch-B crystals should have $\langle h \rangle$ very close to that value. We confirm the low-temperature CE state through the CEA FM reflection [Fig. 2(i)] by neutron diffraction in a slightly larger nonreentrant crystal. A minor part of batch-B crystals may transform into the AAFM below ~ 100 K [Fig. 2(j)]. Others [7, 10] have identified a weak CE superlattice peak at low temperatures which decays upon warming to above ~ 50 K, but then reappears as a strong peak at ~ 120 K. This has the appearance of a nonequilibrium “quenched-in” CE state, that is then annealed out upon warming to ~ 50 K. To dispel this possibility and address thermodynamic stability, we monitor these reflections during slow cooling ($\lesssim 1$ K/min) that should minimize quenched-in CE -order due to sluggish kinetics. We find that the CEA FM reflection is reversible upon slow heating [Fig. 2(i)], and conclude that the CE phase is the low temperature ground state in a majority of each batch-B crystal.

For batch-B crystals, the succession of states with decreasing temperature (shown schematically in Fig. 4) can be cast in terms of entropy. Transforming from the PMI to a charge-ordered paramagnet (CEPM) gains orbital and charge order while the onset of AF in the CE state (CEA FM) at ~ 130 K additionally gains magnetic order. Transitions between the AAFM and CEA FM states are more complex: the internal energy for a CEA FM increases as h deviates from 0.5 while the broad hysteresis implies similar temperature dependencies of their free energies. Therefore the phase boundary is almost vertical versus h . Batch-A crystals also transform from PMI to CEPM at ~ 200 K but CE order appears to be metastable at lower temperatures (dashed lines in Fig. 4) until it transforms at ~ 100 K to the AAFM ground

state. Within this metastable region, the *CE* state develops CEA FM magnetic order below ~ 130 K due to a gain in magnetic entropy. Upon warming, CEA FM order is absent and AAFM order persists until CEPM order is thermodynamically stable ($T > 130$ K). Thus it appears that the magnetic entropy gain in the CEPM is necessary to overcome the barrier between AAFM and *CE* states upon warming.

Batch-*C* crystals show no evidence in conductivity or high-energy x-ray diffraction for *CE* order although they were made with a nominal composition of $x = 0.5$. The *CE* superlattice reflections seen in batch-*A* and batch-*B* crystals were missing at all temperatures down to 100 K. Curiously, all previously published conductivity data [4, 6, 8, 11] and in particular [18] known to us for nominal $x = 0.5$ look more like our batch-*C* crystals, although some show a small hysteresis [4, 6, 8]. A resistivity comparison [19] among these indicates a remarkable consistency in temperature dependence and thus establishes our batch-*C* crystals as a commonly seen variant of the nominal $x = 0.5$ layered manganite. The data of Refs. [6, 8] do show a somewhat larger resistivity peak at ~ 180 K that could be the signature of some *CE*-order in their crystals and each of these report the *CE* reflection. However, the resistivity peak associated with *CE* order in our batch-*A* crystals is at least 10 times larger than the maximum value reported by others [6, 8]. This may imply *CE* order occurs in a larger fraction of our purified batch-*A* crystals.

The electronic nature of AAFM states near $h = 0.5$ is not so easily determined. Conductivity for $x = 0.58$ crystals indicate ab-plane metals [20], whereas insulating behavior is seen for $x = 0.46$ [21]. Conductivity data for the AAFM states of batch-*A* and batch-*C* crystals fall between these two extremes. A possible scenario is a continuous ab-plane-metal to insulator transition as h decreases from ~ 0.58 to ~ 0.46 . In this picture the *CE* order replaces the AAFM over a limited h -range centered at 0.5, but the h -dependence of the AAFM states are otherwise unaffected.

In summary, contrary to published data and accepted wisdom for $\text{LaSr}_2\text{Mn}_2\text{O}_7$, we show that the zero-temperature ground state is the *CE* type predicted by Goodenough [3]. We also find no evidence of *CE* and AAFM coexistence. That we do not know the exact h -values is not critical to these two new observations, but compositional purity was crucial to these discoveries. It was accomplished by stringent testing of small (~ 1 mg) crystals and verified by our observations with bulk probes of only three, *unique* states in the 12 crystals tested. The lack of sufficient purity could explain why others consistently see coexistence of *CE* and AAFM order.

The authors thank Peter Lee for assistance with synchrotron x-ray diffraction at the Advanced Photon Source. This research was supported by the U.S. De-

partment of Energy, Basic Energy Sciences-Materials Sciences, under contract No. DE-AC02-06CH11357.

* Electronic address: KenGray@anl.gov

- [1] S. Jin, T. H. Tiefel, M. McCormack, R. A. Fastnacht, R. Ramesh, and L. H. Chen, *Science* **264**, 413 (1994).
- [2] Y. Moritomo, A. Asamitsu, H. Kuwahara, and Y. Tokura, *Nature* (London) **380**, 141 (1996).
- [3] J.B. Goodenough, *Phys. Rev.* **100**, 564 (1955).
- [4] M. Kubota, H. Yoshizawa, Y. Moritomo, H. Fujioka, K. Hirota, and Y. Endoh, *J. Phys. Soc. Japan* **68**, 2202 (1999).
- [5] C.D. Ling, J.E. Millburn, J.F. Mitchell, D.N. Argyriou, J. Linton, and H. Bordallo, *Phys. Rev. B* **62**, 15096 (2000).
- [6] D.N. Argyriou, H.N. Bordallo, B.J. Campbell, A.K. Cheetham, D.E. Cox, J.S. Gardner, K. Hanif, A. dos Santos, and G.F. Strouse, *Phys. Rev. B* **61**, 15269 (2000).
- [7] T. Chatterji, G.J. McIntyre, W. Caliebe, R. Suryanarayanan, G. Dhaleene, and A. Revcolevschi, *Phys. Rev. B* **61**, 570 (2000).
- [8] T. Kimura, R. Kumai, Y. Tokura, J.Q. Li, and Y. Matsui, *Phys. Rev. B* **58**, 11081 (1998).
- [9] Y. Wakabayashi, Y. Murakami, I. Koyama, T. Kimura, Y. Tokura, Y. Moritomo, Y. Endoh, K. Hirota, *J. Phys. Soc. Japan* **72**, 618 (2003).
- [10] S.B. Wilkins, P.D. Spencer, T.A.W. Beale, P.D. Hatton, M. v. Zimmermann, S.D. Brown, D. Prabhakaran, and A.T. Boothroyd, *Phys. Rev. B* **67**, 205110 (2003).
- [11] Y. Tomioka and Y. Tokura, *Colossal magneto-resistive oxides* (Gordon Breach, Amsterdam, 2000), Chap. 8.
- [12] J.Q. Li, Y. Matsui, T. Kimura, and Y. Tokura, *Phys. Rev. B* **57**, R3205 (1998).
- [13] J.Q. Li, C. Dong, L.H. Liu, and Y.M. Ni, *Phys. Rev. B* **64**, 174413 (2001).
- [14] Z.P. Luo, D.J. Miller, and J.F. Mitchell, *Phys. Rev. B* **71**, 014418 (2005).
- [15] J.F. Mitchell, D.N. Argyriou, J.D. Jorgensen, D.G. Hinks, C.D. Potter, and S.D. Bader, *Phys. Rev. B* **55**, 63 (1997).
- [16] Qing'An Li, K.E. Gray, and J.F. Mitchell, *Phys. Rev. B* **59**, 9357 (1999).
- [17] Qing'An Li, K.E. Gray, S. Nyborg Ancona, H. Zheng, S. Rosenkranz, R. Osborn, and J.F. Mitchell, *Phys. Rev. Lett.* **96**, 087201 (2006).
- [18] X.J. Chen, C.L. Zhang, J.S. Gardner, J.L. Sarrao, and C.C. Almasan, *Phys. Rev. B* **68**, 064405 (2003).
- [19] To compare the literature results on an equivalent basis, we use our own four-terminal data, along a flat c -axis face of the crystal that is the "top" voltage in Fig. 3(a) and Ref. [16]. We assume this configuration for cases in the literature where the lead configuration is unspecified.
- [20] E. Badica, K.E. Gray, J.F. Mitchell, and H. Zheng, *Phys. Rev. B* **70**, 174435 (2004).
- [21] Qing'An Li, K.E. Gray, and J.F. Mitchell, *Phys. Rev. B* **67**, 184426 (2003). N.B. The crystal used in this study was originally designated as $x = 0.48$, but extensive recent studies using boules made nominally at $x = 0.48$ and 0.46 lead us to believe it was actually closer to 0.46.